Sorption of Biphenyl in Nonacidic Faujasitic Y Zeolites: Modeling and Spectroscopic Studies

Isabelle Gener, Gabrielle Ginestet, Guy Buntinx, and Claude Brémard*

Laboratoire de Spectrochimie Infrarouge et Raman UMR-CNRS 8516, Centre d' Etudes et de Recherches Lasers et Applications, Bât. C5 Université des Sciences et Technologies de Lille, 59655 Villeneuve d'Ascq Cedex, France

Received: September 15, 1999; In Final Form: March 27, 2000

The predictions of the sorption energy, sorption site, conformation, mobility, and vibrational spectra of biphenyl (BP, $C_{12}H_{10}$) occluded in nonacidic faujasitic Y zeolites $M_n(SiO_2)_{192-n}(AlO_2)_n$ (M_nFAU, $n = 0$ or 56 and M $= Na^+$, K^+, or Cs^+) were carried out using Monte Carlo simulations (MC), molecular mechanics (MM), and molecular dynamics (MD) calculations. The zeolite−biphenyl interactions have been tuned by varying the aluminum content *n*, the charge-balancing cation M^+ of the zeolite, and the BP loading. No preferential sorption site was expected in purely siliceous FAU at 300 K, whereas well-defined location sites energetically favored were expected in $M_{56}FAU$ aluminated faujasite. BP lies in the cavity in a twisted conformation with one phenyl group facially coordinated to the SII cations and the other phenyl group engaged in the 12-ring windows. The accommodation of two BPs within the same supercage occurs at relatively low coverage (2 BP/UC) and is hindered by the M^+ size. The diffuse reflectance UV−visible absorption data indicate the occupancy of 2 BP per supercage at bulk loading higher than 1 BP/UC. Surprisingly, the BP mean-square displacements (MSD) was found to be slightly lower in FAU than in $Na_{56}FAU$, although the intracage mobility was found to be higher, while the BP MSD was found to be lower with bulky M^+ cations. The calculated vibrational densities of states of the atoms of the framework, M^+ and BP, were found to be in reasonable agreement with the frequency values deduced from the IR absorption and Raman scattering spectra of BP-loaded M_nFAU, bare M_nFAU, and free BP. These results indicate no marked constraint between host and guest even at high BP coverage. The BP rapid motions average the microenvironments and vibrational couplings as found in solution. The experimental conditions of the BP sorption and the Ar, He, or O_2 gas pressure do not induce significant changes of occluded BP characteristics.

Introduction

The synthetic faujasite analogues, zeolites X and Y, both differing only in the Si/Al ratio, are used extensively as catalysts in a variety of reactions and separation processes. The acidic nature of highly siliceous faujasites is largely exploited in hydrocracking. The sorption into inorganic molecular sieves such as zeolite Y can provide an efficient way to remove and photodegrade organic pollutants such as polychlorinated biphenyls (PCBs) and polyaromatic hydrocarbons (PAHs).[1] Several aspects of the photophysics and photochemistry of occluded aromatics have been revealed recently.[2−6]

Earlier, the sorption sites, energetics, and dynamics of aromatics such as benzene and xylenes within the void space of faujasitic zeolites were extensively investigated experimentally by thermodynamic measurements,[7,8] neutron and X-ray diffraction,[9−13] NMR,[14−18] inelastic neutron scattering (INS),[19] quasi elastic neutron scattering (QENS),[20] and UV−visible,[21] infrared absorption,[22−24] and Raman scattering.[25] The computer calculations back the experimental results because they are able to resolve the structure, energetics, and dynamics of guest molecules at the atomic scale.[26−34] In addition, the calculations can simulate some aspects of the spectroscopic data.

No such data are available for the biphenyl (BP) occluded in faujasitic zeolites, so the computer simulations can provide informative predictions concerning the conformation, sorption sites, energetics, and dynamics of BP within the void space of faujasitic zeolites.[5] The UV−visible, IR absorption, and Raman scattering spectrometries have been reported previously to provide valuable information concerning the molecular structure, sorption site, interactions, and chemical reactions of the guest molecules within the void space of porous materials.[35,36]

In this paper, we present the prediction of the sorption energy and sites, conformation, mobility, and vibrational motions of BP occluded in nonacidic faujasitic Y zeolites $M_n(SiO_2)_{192-n}(AlO_2)_n$ (M_nFAU, $n = 0$ or 56 and M $= Na^+$, K^+, or Cs^+) using Monte Carlo simulations (MC), energy minimization (MM), and molecular dynamics (MD) calculations. The diffuse reflectance UV−visible absorption, IR absorption, and Raman scattering investigations of BP sorption are expected to provide structural and dynamic evidence. The zeolite−biphenyl interactions have been tuned by varying the aluminum content *n*, the charge-balancing cation M^+ of the zeolite, and the BP loading and experimental conditions of the sorption.

Experimental Section

Materials. The completely siliceous FAU or USY zeolite $(SiO_2)_{192}$ (Si/Al = 100) was kindly provided by Degussa. The $Na_{56}FAU$ or $Na_{56}Y$ zeolite $Na_{56}(SiO_2)_{136}(AlO_2)_{56}$ (Si/Al = 2.49) was obtained from Union Carbide. The Na^+ cations of Na_{56}-FAU were exchanged with K^+ and Cs^+ cations to give $Na_4K_{52}(SiO_2)_{136}(AlO_2)_{56}$ and $Na_5Cs_{51}(SiO_2)_{136}(AlO_2)_{56}$ samples. The exchange was carried out according to a processes reported

10.1021/jp993291a CCC: $19.00
Published on Web 11/16/2000

previously.[37] All the zeolite samples were used after a calcination procedure. Biphenyl, $C_{12}H_{10}$ (Merck-Schuchardt), was used after a dehydration procedure. Pure and dry Ar and O_2 gasses were used.

Sorption of Biphenyl. Weighted amounts (∼1.4 g) of powdered hydrated zeolite $M_n(SiO_2)_{192-n}(AlO_2)_n$ (1−2 μm particle size) were introduced into an evacuable heatable silica cell. The sample was dried under vacuum (10^{-3} Pa) and heated stepwise to 773 K under air. O_2 was then admitted into the cell for 6 h at 773 K. The thermal treatment removed the water content and the organic impurities completely.[37] The crystallinity of the samples was checked by XRD and was not reduced by this treatment.[37] Then the sample was held under vacuum and cooled to room temperature under dry argon. Weighted amounts of bisublimated BP, corresponding to 1−16 BP per $M_n(SiO_2)_{192-n}(AlO_2)_n$ unit cell, were introduced into the cell under dry Ar, and the powder mixture was shaken. After four weeks at 323 K, the sample was held under vacuum for 3 h and then transferred under dry argon either in a quartz glass Suprasil cuvette for FT-Raman and diffuse reflectance UV−visible experiments or in a cell equipped with CaF_2 windows for diffuse reflectance IR measurements.

Instrumentation. The elemental analyses (C, H, Al, Si, Na, K, and Cs) of the bare and loaded zeolites were obtained from the Service Central d' Analyse du Centre National de la Recherche Scientifique (Vernaison, France).

The UV−visible diffuse reflectance spectra of the sample were recorded between 200 and 850 nm using a Cary 3 spectrometer equipped with an integrating sphere. The corresponding bare zeolite was used as the reference. Conventionally, an equation derived from the Kubelka−Munk phenomenogical theory[38] is used in order to relate a chromophore concentration for the intensity of the sample diffuse reflection. In the equation $F(R) = (1 - R)^2/2R = K/S$, the sample is treated as a continuum; R represents the ratio of the diffuse reflectance of the loaded zeolite to that of the dehydrated neat zeolite, K designates an absorption coefficient proportional to the concentration of the chromophore, and S represents the scattering coefficient of the powder.

A Bruker IFS 88 instrument was used as a near-IR FT-Raman spectrometer with a continuous-wave Nd:YAG laser operating at 1064 nm as the excitation source. A 100−200 mW laser was used. The spectra (3500−150 cm^{-1}) were recorded at 2 cm^{-1} resolution using 600 scans. The Opus Bruker software was used for spectral acquisition, data treatment, and plotting.

The FTIR spectrometer was a Bruker IFS 113 V instrument equipped with a liquid-nitrogen-cooled MCT detector (Mid-IR) with the suitable beam splitter. The OPUS Bruker software was used for spectral acquisition, storage, manipulation, and plotting. The spectra were recorded at 2 cm^{-1} resolution. The in situ diffuse reflectance apparatus is a Harrick Scientific Diffused Reflectance Attachment "DRA-2CI" praying mantis and "HVC-DRP" cell equipped with CaF_2 windows.[39] The Kubelka−Munk function was used in order to relate the chromophore concentration to the intensity of the sample diffuse reflection. The program Cerius[2] (version 3.8) was established on a Silicon Graphics workstation.

Model: Structure and Force Field. The atomic positions for the zeolite hosts FAU, Na_{56}FAU, K_{56}FAU, and Cs_{56}FAU were obtained from all the available X-ray or neutron diffraction determinations of the structures.[40,9,41,42] The substitional Si/Al disorder was applied according to the Loewenstein rule.[43] The partial occupancy of extraframework cation sites was taken into account explicitly in view of the extensive structural work published in the literature. The framework is composed of a cubo-octahedral arrangement of six-membered rings of O atoms to form 13-Å diameter large cavities called supercages. The supercages are interconnected by 8-Å diameter 12-ring windows consisting of 12 Si/Al and 12 O atoms. One unit cell, containing eight supercages, is used to construct the host simulation box. The resulting host systems consist of 192 Si, 384 O, and 192 Si/Al atoms for FAU and 384 O and 56 M^+ atoms for M_{56}-FAU. The partial atomic charges of the zeolite atoms were taken from previous works.[35,42,44] FAU: Si, +1.6; O, −0.8. M_{56}FAU: Si, +1.42; Al, +1.23; O, −0.85; M, +1. The geometrical parameters of BP and the partial atomic charges are derived from ab initio calculations or X-ray determination.[45−50]

TABLE 1. Lennard−Jones Parameters for Guest Molecule−Faujasitic Zeolite Short-Range Nonbonded Interactions

atom pair	$A_{\alpha\beta}$ (kJ mol^{-1} Å^{12})	$B_{\alpha\beta}$ (kJ mol^{-1} Å^{6})	ref
C···C	4627406	2712	56
H···H	71891	133	56
Ar···Ar	9796197	6244	56
O···O	1155882	1446	56
Na···Na	38844	246	55
K···K	1377460	899	57
Cs···Cs	5008978	1939	57
O_z[a]···Na	737477	6040	55
O_z[a]···K	1228732	1250	
O_z[a]···Cs	2400110	1860	
O_z[a]···C	2263524	3114	
O_z[a]···H	250152	831	
Na···H	103258	229	
Na···C	1289784	953	
K···H	313914	347	
K···C	2557884	1572	
Cs···H	590245	506	
Cs···C	4957229	2328	

[a] O_z represents the oxygen atoms of the zeolite framework.

The potential energy E of the simulated zeolite−sorbate (Z−S) system is calculated by the summation of four terms: the bonded interaction energy of Z, E_Z; the bonded interaction energy of S, E_S; the nonbonded interaction energy between Z and S, E_{ZS}; and the nonbonded interaction energy between S and S, E_{SS}. The force field values (bond, angle, and torsion) help determine the V_Z term derived from ab initio calculations of small model systems.[51,52] The force field values for calculating the E_S, E_{ZS}, and E_{SS} terms are derived from previous works.[53−57] The sum of a Coulomb potential and a Lennard−Jones (L−J) potential is used to describe the nonbonded interactions. The L−J potential accounts for repulsive $A_{\alpha\beta}/r_{ij}^{12}$ and dispersive $-B_{\alpha\beta}/r_{ij}^{6}$ interactions (the parameters are listed in Table 1 as $A_{\alpha\beta}$ and $B_{\alpha\beta}$). The short-range L−J interactions with Si and Al are ignored because they are well shielded by the O atoms of the framework (Table 1).

Calculations. The modeling results published herewith were generated using the program Cerius[2] (version 3.8) developed by Molecular Simulations Incorporated.

In the Monte Carlo simulations, the Si, Al, and O atoms of the zeolite framework and Na^+ cations are fixed at the crystallographic coordinates determined from structural data. The BP structure is assumed to be rigid. The MC simulations at fixed loading were carried out at 300 K using the conventional Metropolis algorithm based on the configurational energy change

$$P = \min[1; \exp(-\Delta E/kT)] \qquad (1)$$

where P is the probability of the move being accepted, $\Delta E = \Delta(E_{ZS} + E_{SS})$ is the energy change between the new configu-

ration and the previous configuration, k is the Boltzmann constant, and T is the temperature of the simulation. To eliminate the effect of boundaries, we have used periodic boundary conditions with a period equal to one zeolite unit cell. A cutoff radius of 15 Å is applied to the Lennard−Jones interactions, and the long-range electrostatic interactions are calculated using the Ewald summation technique. The simulation takes a number of steps to equilibrate from its original random position. For accurate statistical results, the steps made prior to equilibration should be excluded from the analysis. One typical MC run took 1.5 million steps.

The Monte Carlo simulations of the sorption and cosorption at fixed pressures were carried out using the grand canonical ensemble (GCMC); in this method, the number of particles in the system is determined by the fixed chemical potential of each species. One Monte Carlo step consists of four parts (create, destroy, translate, and rotate a molecule). The basis of the simulation is as follows:

(i) Equilibrium is achieved when the temperature and the chemical potential of the gas inside the framework are equal to the temperature and the chemical potential of the free gas outside the framework.

(ii) Create: A random molecule is picked from the list of sorbates, placed in a random position, and orientation in the framework. The new configuration is accepted with probability P

$$P = \min[1; \exp(-\Delta E/kT - \ln(N_i + 1)kT/f_i V)] \qquad (2)$$

where P, ΔE, k, and T were defined above, N_i is the current number of molecules of component i in the framework, f_i is the fugacity of component i in the gas phase (assumed to be 1), and V is the cell volume.

(iii) Destroy: The simulation randomly chooses which sorbate type to remove and then randomly chooses a molecule of that type in the framework. The new configuration is accepted with probability P

$$P = \min[1; \exp(-\Delta E/kT + \ln N_i kT/f_i V)] \qquad (3)$$

(iv) Translate: A sorbate molecule in the framework is chosen at random and translated by a random amount within a cube of size 2δ (where δ is the maximum step size). The new configuration is accepted with probability P. The acceptance criterion is the same as that for the fixed loading simulation (see above).

(v) Rotate: A sorbate molecule is chosen in the framework. The rotation axis is chosen at random, and the molecule is rotated by a random amount within the range $-\theta$ to $+\theta$ (where θ is the maximum step size). The new configuration, based on the energy change, is accepted with the same probability applied to the translation move above. The simulation takes a number of steps to equilibrate from its original random position. For accurate statistical results, the steps made prior to equilibration should be excluded in the analysis. One typical GCMC run took from 2−3 million steps. From each sorption trajectory file, a histogram of the energy distribution for each sorbate is plotted. In the mass-cloud analysis, the center-of-mass of each sorbate in each configuration is displayed as a dot in the model space.

In the molecular mechanics (MM) and molecular dynamics (MD) simulations, the time-consuming Ewald summation is not performed, and the electrostatic and (L−J) interaction cutoffs are defined by two parameters: the spline-on and the spline-off distances. Within these ranges, the nonbonded interaction energy is attenuated by the spline function. Beyond the spline-off distance, nonbonded interactions are ignored. The spline-on and spline-off distances are taken to be 15 and 30 Å for the electrostatic and (L−J) interactions, respectively. At first, simulated annealing is performed from the last configuration of the MC simulations following by the energy minimization of $E = E_Z + E_S + E_{ZS} + E_{SS}$ using the conjugate gradient minimization procedure (MM). The Si, Al, and O atoms of the zeolite framework and the BP structure were taken to be flexible, and Na^+ cations were taken to be mobile.

The MD simulations were performed at 300 K in the NVE ensemble for 100 ps ($E = E_Z + E_S + E_{ZS} + E_{SS}$). The equations of motions were integrated by using the velocity form of the Verlet algorithm with a time step of 0.2 fs. The guest molecule coverage corresponds to 1 BP per unit cell (UC). The densities of vibrational states of the individual atoms of zeolite (Si, Al, O, and M^+) and sorbate (C and H) were calculated by Fourier transformation of the corresponding velocity autocorrelation function. We performed extended MD runs over additional periods from 0.5 to 1 ns with a time step of 2 fs for coverage between 1 and 8 BP/UC with fixed-framework (Si, Al, and O) mobile M^+ cations and flexible BP. From the trajectory file, we calculated the mean-square displacement as well as radial distribution functions.

Validation of the Model and Calculation Approximations. The behavior of benzene in siliceous FAU and Na_{56}FAU faujasite is well documented, and many observations and models are available in the literature. So the structure, sorption sites, energetics, dynamics, and vibrational properties of benzene occluded in FAU and Na_{56}FAU[9] were recalculated using the force field displayed above in order to valid the set of parameters used and the calculation approximations. We would like to point out that the polarizability interactions between the sorbate and zeolite atoms are not taken into account explicitly. Explicit treatment of polarization should be included through the introduction of an induction term[58] or through the computation of the partial charges themselves according to their own equations of motions dynamic variables.[59] These two approaches have been very time-consuming, and therefore, the explicit treatment of polarization is usually assumed to be weak and avoided for occluded aromatics in a first approximation.[27−34]

The heats of sorption and the location sites of benzene were accurately reproduced through Monte Carlo simulations with the set of parameters used in the present work.[9,60] The error made by fixing the cation positions throughout the calculations is therefore assumed to be negligible. The relaxation of all the structural parameters in the subsequent energy minimization procedure did not induced marked changes of the structural parameters. In the adsorption of hydrophobic molecules such as benzene, the extraframework cation motion was found to be negligible. Fitch et al. reported a shift of 0.009 nm for Na^+ cations in Na_{56}FAU due to the interaction of benzene.[9]

The IR absorption spectra of benzene and zeolite were reasonably reproduced through MD calculations and subsequent Fourier transformation of the autocorrelation function of the dipole moment of the system. We performed extended MD runs over additional periods from 0.5 to 1 ns with a time step of 2 fs for 1 C_6H_6/UC with fixed frameworks (Si, Al, and O), mobile M^+ cations, and rigid C_6H_6. Estimates of diffusion coefficients of benzene in siliceous FAU and Na_{56}FAU—10^{-10} and 10^{-11} $m^2\ s^{-1}$, respectively—were found to be in reasonable agreement with the ^2H NMR experimental values—4×10^{-10} and 4×10^{-12} $m^2\ s^{-1}$, respectively.[14,16]

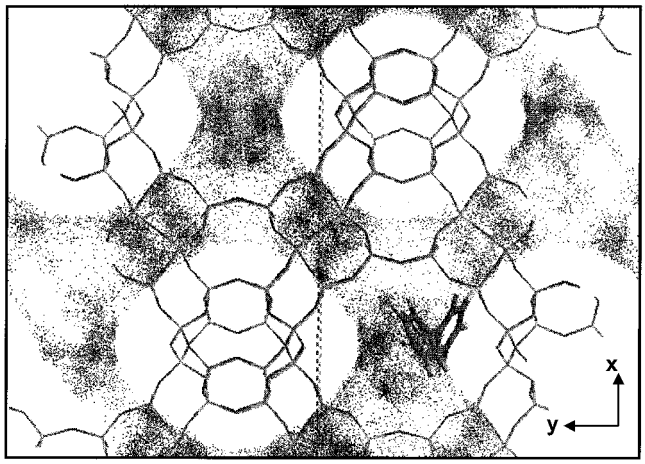

Figure 1. Probable positions of the center-of-mass of BP in the void space of the siliceous faujasite FAU at low coverage (1 BP/FAU) with sorption energy in the −[90, 105 kJ mol^{-1}] range. The black dots represent the centers-of-mass. The black and shaded sticks represent the O and Si atoms of the $(SiO_2)_{192}$ framework, respectively. The white and shaded cylinders represent the H and C atoms of the $C_{12}H_{10}$ molecule, respectively.

The models of the structures, force field, and localized charges and the approximations made to reduced the computing time were found to be reasonable for simulating some experimental features of occluded benzene and appear to be suitable for predicting the behavior of biphenyl within the void space of faujasitic zeolites.

Results and Discussion

1. Monte Carlo Simulations. The predictions of the energies and sites of sorption of rigid BP in fixed M_nFAU were carried out at 300 K and constant loading from 1 to 16 BP/UC by Monte Carlo simulations using the conventional Metropolis algorithm and at saturation using the grand canonical algorithm at constant BP pressure (10 kPa). The calculations took into account the nonbonded interaction energy between the zeolite (Z) and the sorbate (S), E_{ZS}, and the nonbonded interaction energy between S and S, E_{SS} (see Experimental Section)

$$E_{ZS} + E_{SS} = \sum_{ij} A_{\alpha\beta}/r_{ij}^{12} - B_{\alpha\beta}/r_{ij}^{6} + q_i q_j / r_{ij} \qquad (4)$$

Biphenyl Occluded in FAU. At 1 BP/FAU loading, the average sorption energy is found to be approximately -96 ± 4 kJ mol^{-1} and then decreases slightly as the loading increases to approximately -134 ± 8 kJ mol^{-1} at 16 BP/FAU. The saturation of FAU occurs at ∼16 BP/FAU. No supplementary attempts were made to predict the BP sorption isotherm without any biased scheme or experimental counterpart. The distribution of an individual BP molecule's lowest sorption energy and the distribution of positions occupied by the BP center-of-mass according to the lowest energy provide pertinent findings, shown in Figures 1 and 2, respectively.

At very low coverage—namely, 1 BP/FAU—the distribution of individual BP energy exhibits a maximum at −96 kJ mol^{-1} (Figure 1). The distribution of positions occupied in the void space by 1 BP/FAU with an energy close to −96 kJ mol^{-1} is large (Figure 2). The absence of well-defined sorption sites indicates that the net potential surface accessible to the molecules is fairly uniform. This finding is consistent with benzene sorption modeling and the inability to locate the C_6H_6 sorbate in FAU by neutron diffraction.[40] Nevertheless, it is apparent that the probability of the presence of BP is significantly higher in the vicinity of the windows.

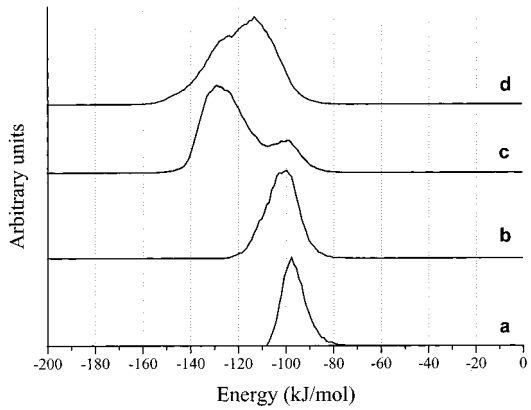

Figure 2. Distribution of calculated energies of BP molecules in $(SiO_2)_{192}$ siliceous faujasitic Y (FAU) zeolite at 300 K for (a) 1, (b) 2, (c) 4, or (d) 8 BP per unit cell.

The sorption energy decreases gradually as the loading increases before the saturation (Figure 1). The distributions of positions occupied by the BP center-of-mass corresponding to these energies provide no evidence of preferred well-defined sorption sites at 300 K. The lowering of the sorption energy at high coverage indicates a significant sorbate−sorbate interaction energy contribution and the accommodation of two BP per supercage even at relatively low coverage. A comparison can be made with the experimentally determined sorption heat of benzene in FAU zeolite as a function of loading that was found to increase at 323 K from 53 to 60 kJ mol^{-1} in the range of 2−20 benzene per unit cell.[60]

Biphenyl Occluded in M_{56}FAU ($M^+ = Na^+$, K^+, or Cs^+). At 1 BP/M_{56}FAU loading, the corresponding average sorption energy values were found to be approximately −105 kJ mol^{-1} ($M = Na^+$), −88 kJ mol^{-1} ($M = K^+$), and −109 kJ mol^{-1} ($M = Cs^+$). The trend, as a function of M^+ content, clearly reflects the increasing importance of strong cation−sorbate interactions as the aluminum content increases. This finding is in agreement with previously reported corresponding results concerning benzene.[60,61] The distribution of the BP center-of-mass positions indicates the presence of well-defined sorption sites that are consistent with the well-defined location of the C_6H_6 sorbate in Na_{56}FAU found by neutron diffraction and simulations.[9,27−34] The increases of sorption energy and the BP location in the vicinity of Site II indicate the effect of BP with M^+ interactions. In addition, the aluminum content induces the increase of the basicity of the oxygen atoms. This effect is interpreted in the modeling through a relatively higher partial charge on oxygen.

At 1 BP/Na_{56}FAU, the distribution of each BP molecule's lowest sorption energy is centered around approximately −105 kJ mol^{-1}. The sorption energy decreases gradually as the loading increases before the saturation while the distributions broaden. At 16 BP/Na_{56}FAU, the distribution is centered at −135 kJ mol^{-1}, with a bandwidth around 40 kJ mol^{-1}, Figure 3.

The lowering of the sorption energy at high coverage indicates a significant sorbate−sorbate interaction energy contribution. The distribution of BP positions indicates the accommodation of 2 BP per supercage even at relatively low coverage. For exemple, the filling of the 8 empty supercages of the unit cell with 8 BP was not found to be homogeneous. Several supercages contain 2 BP, whereas some supercages contain 1 BP and some remain empty. This latter simulated cage occupation results is in accurate agreement with nonuniform occupation of the

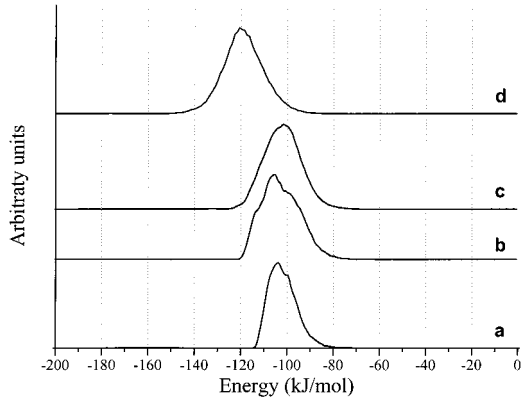

Figure 3. Distribution of the calculated energies of BP molecules in $Na_{56}(AlO_2)_{56}(SiO_2)_{136}$ faujasitic Y (Na_{56}FAU) zeolite at 300 K for (a) 1, (b) 2, (c) 4, or (d) 8 BP per unit cell.

supercages by aromatics as deduced from fluorescence emission spectroscopy.[62]

Biphenyl and Argon or Oxygen Occluded in Na_{56}FAU. To evaluate the effects of the cosorption of argon or oxygen gas upon the BP sorption sites, we carried out the prediction of the BP and Ar cosorption using the grand canonical algorithm at 10 kPa BP equilibrium pressure and 110 kPa Ar pressure. The energetics and structural characteristics of BP were found to be analogous to the corresponding characteristics simulated through BP sorption alone. Analogous results were obtained for BP and O_2 cosorption.

2. Molecular Mechanics Calculations. *BP/FAU.* Taking into account that the net potential surface of siliceous FAU accessible to the BP molecules is fairly uniform, we found several sorption sites with twisted BP conformation through energy minimization procedures.

BP/M_{56}FAU ($M^+ = Na^+$, K^+, or Cs^+). The energy minimization procedure ($E = E_Z + E_S + E_{ZS} + E_{SS}$) of the system 1 BP/$M_{56}$FAU was carried out with all the structural parameters of host and sorbate relaxed. The results are representative of the expected structures at absolute zero and predict the preferred conformation of BP occluded in the porous void of the M_{56}-FAU zeolites as well as the framework deformation and M^+ extraframework displacement. The energy minimization of 1 BP/M_{56}FAU localized within a supercage generates very weak deformations of the framework and weak deformations of BP. The repartition of the internal energy, van der Waals energy, and electrostatic energy indicates the major role of the electrostatic interactions, particularly through the M^+ phenyl group interactions. For M = Na^+, K^+, or Cs^+, BP was found to lie in the supercage with a phenyl group facially coordinated to the SII cations and the other phenyl group engaged in the 12-ring windows (Figure 4). For M = Cs^+, one phenyl group of BP is constrained to lie between two Cs^+ cations in site II. The shortest distances $M^+\cdots C$ were found to be 2.9 (Na^+) and 4.3 Å (K^+), and the shortest distances $Cs^+\cdots C$ were found to be 3.9 and 4.3 Å. The values of the dihedral angle obtained after the minimization procedure of the 1 BP/M_{56}FAU systems were found to be ~50° and do not vary markedly from the value calculated for the free molecule (42°). The equilibrium positions of the M^+ cations were found to be analogous to the positions of the corresponding sites of the bare M_{56}FAU (M = Na^+, K^+, or Cs^+).

This structural situation can be compared to that of the most favored sorption site found for C_6H_6 occluded in Na_{56}FAU—the benzene molecules lie facially coordinated to one cation in Site II and in the window.[9]

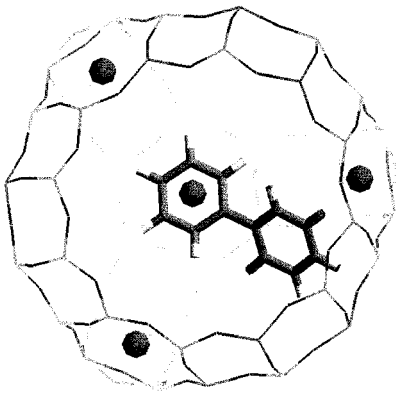

Figure 4. Predicted conformation and sorption site of BP occluded in a supercage of Na_{56}FAU at low coverage (1BP/Na_{56}FAU) resulting from energy minimization. The black and shaded sticks represent the O and Si/Al atoms of the $(AlO_2)_{56}(SiO_2)_{136}$ framework, respectively. The white and shaded cylinders represent the H and C atoms of the $C_{12}H_{10}$ molecule, respectively. The shaded spheres represent the Na^+ cations.

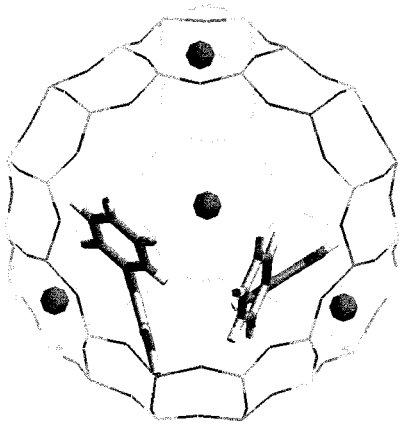

Figure 5. Predicted conformations and sorption sites of 2 BP occluded in a supercage at 8 BP/Na_{56}FAU coverage resulting from energy minimization. The black and shaded sticks represent the O and Si/Al atoms of the $(AlO_2)_{56}(SiO_2)_{136}$ framework, respectively. The white and shaded cylinders represent the H and C atoms of the $C_{12}H_{10}$ molecule, respectively. The shaded spheres represent the Na^+ cations.

The energy minimization of the 4 BP/Na_{56}FAU system indicated the structure of BP pairs occluded in the same supercage (Figure 5). The two BP sorption site geometries were found to be analogous to that obtained for 1 BP per supercage. The bimolecular arrangement appeared to be governed by Na^+—BP interactions rather than BP—BP interactions. The value of the BP dihedral angle was found to be around 50°.

The minimization of the energy of the 16 BP/Na_{56}FAU system with all the structural parameters allowed to be relaxed confirmed the most favorable sites and BP twisted conformation, while the deformations of the host framework were not found to be significant.

3. Molecular Dynamics Calculations. The MD simulations were performed in the NVE ensemble at 300 K with a time step of 0.2 fs over 100 ps, with all the structural parameters relaxed for the BP/FAU and BP/M_{56}FAU systems derived from energy minimization ($E = E_Z + E_S + E_{ZS} + E_{SS}$). Some MD runs were also performed in the NVE ensemble at 300 K with a time step of 2 fs over 1 ns, with mobile M^+ cation and flexible BP in a fixed framework for the BP/FAU and BP/M_{56}FAU systems.

3.1. Radial Distribution Functions. Analysis of the radial distribution functions yields information about the structural characteristics of sorbates and extraframework cations in the

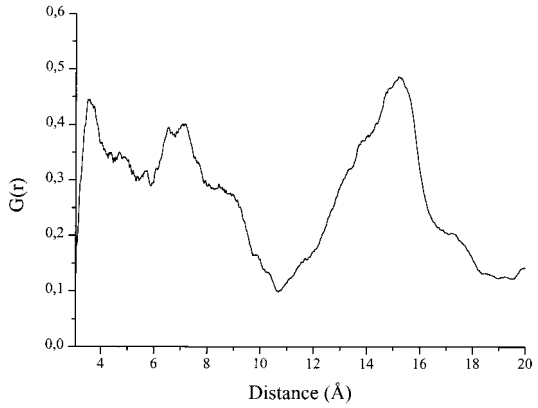

Figure 6. Radial distribution functions $G(r)$ at 300K among the phenyl groups of BP at 1BP/Na_{56}FAU coverage with respect to the Na^+ of the sorption site S(II) (see Figure 2).

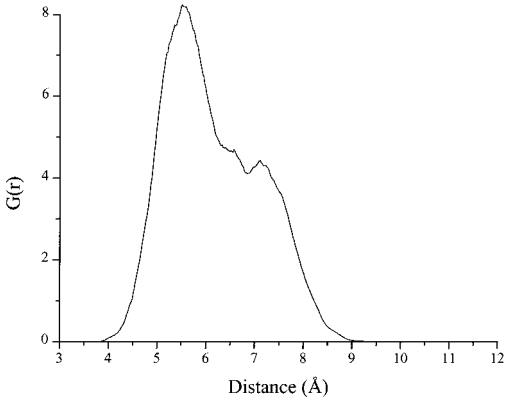

Figure 7. Radial distribution functions $G(r)$ at 300K between the two inter-ring C−C bonds of a BP pair occluded in a supercage at 8 BP/Na_{56}FAU coverage.

pores of zeolites. The radial distribution function $G_{AB}(r)$ is defined as the probability that two centers A and B are separated by a distance r with regard to a statistical distribution of both centers A and B

$$G_{AB}(r) = [N_{AB}(r)V/(N_A N_B - N_{AB})]4\pi r^2 \, dr \qquad (5)$$

with N_A being the number of atoms in group A, N_B the number of atoms in group B, N_{AB} the number of atoms common to both groups A and B, and V the unit cell volume.

BP/FAU. The radial distributions G representative of the BP−BP distances, deduced from the trajectory file performed at 8 BP/FAU loading, provide evidence of the persistence over the simulation time (1 ns) of the BP pairs through a prominent maximum at 5 Å (not shown).

BP/Na_{56}FAU. A selection of the radial distributions after MD calculations over 1 ns concerning the expected BP sorption site at 1 BP/Na_{56}FAU loading is shown in Figure 6. Figure 6 shows the radial distribution function between the Na^+ S(II) and the facially coordinated phenyl group of BP. These data provide evidence of the BP sorption site through the weak G maximum at 3.5 Å and the intracage and intercage BP displacements through the maxima at 7 and 15.2 Å (Figure 6), respectively. The corresponding radial distributions (not shown) deduced from the trajectory file performed at 8 BP/Na_{56}FAU loading yield approximately analogous results. The radial distributions concerning the S(II) Na^+ framework and Na^+−Na^+ distances were found to be analogous, with some weak differences, to the values obtained with bare Na_{56}FAU.

However, the G values representative of the BP−BP distances provide evidence of the persistence over the simulation time (1 ns) of the BP pairs through a prominent maximum at 5.5 Å (Figure 7).

3.2. Velocity Autocorrelation Functions and Spectral Densities. Time correlation functions and their Fourier transforms are useful tools for examining the dynamic properties of host−guest systems. In this section, we analyze the velocity autocorrelation functions (VACF) $C_{vv}(t)$ and the corresponding Fourier transformation, which was calculated as previously reported

$$C_{vv}(t) = \langle v(t)v(0)\rangle/\langle v(0)v(0)\rangle \qquad (6)$$

BP/FAU. The Fourier transformation of VACF provides the vibrational density of states of the framework and BP. In the trajectory file obtained for 1 BP/FAU loading with a time step of 0.2 fs over 100 ps, the Fourier transformations of the VACF of framework atoms exhibit spectral densities (not shown) which were found to be very similar to those obtained for the bare zeolite and in agreement with those of the Raman bands assigned to the framework.

The atomic vibrational density of states (2 cm^{-1} resolution) of BP occluded in FAU exhibits features in agreement with those of the experimental Raman and IR bands (see below the experimental results). It should be noted that all the vibrational modes were found to be in the expected wavenumber ranges and backed the validity of our results. Particularly, the vibrational density of state calculated at room temperature for the C−C inter-ring atoms of 1 BP/FAU exhibits a peak at 1285 cm^{-1}. These calculated data will be compared with the Raman results and discussed in section 6.1.

BP/Na_{56}FAU. The Fourier transformation of VACF provides the vibrational density of states of the framework, Na^+ and BP. From the trajectory file obtained for 1 BP/M_{56}FAU loading with a time step of 0.2 fs over 100 ps, the Fourier transformations of the VACF of framework and extraframework atoms exhibit spectral densities (not shown) that were found to be very similar to that obtained for the bare zeolites. The vibrational density of states (2 cm^{-1} resolution) of the 1 BP occluded in Na_{56}FAU is shown in Figure 8 and will be compare to the experimental Raman and IR spectra (see the experimental results below). It should be noted that all the vibrational modes were found to be in the expected wavenumber ranges and backed the validity of our results.

Particularly, the vibrational density of state calculated at room temperature for the C−C inter-ring atoms of 1 BP/Na_{56}FAU exhibits a peak at 1285 cm^{-1}. These calculated data will be compared with the Raman and IR results and discussed in section 6.1. The increases of the BP loading do not provide marked changes in the BP vibrational density of states.

3.3. Mechanism of Self-Diffusion. The MD simulations were performed for 1 ns with flexible BP in a fixed FAU framework or a fixed M_{56}FAU framework with mobile M^+ cations. From the trajectory file, we calculated the mean-square center-of-mass displacements. Sorbate intracrystalline self-diffusion coefficients at 300 K can be calculated from the mean-square displacement (MSD) $\Delta R(t)^2$ for the specified atoms of BP using the Einstein relation

$$D = 1/6t\langle \Delta R(t)^2 \rangle \qquad (7)$$

The averaging takes place over time origins spaced by 5 ps and over all guest molecules.

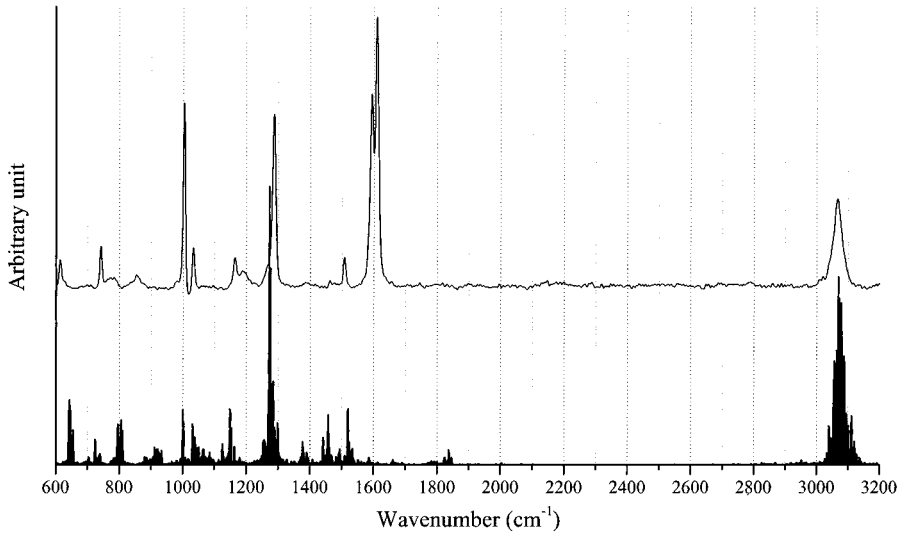

Figure 8. Vibrational density of state (bottom) and Raman spectrum (top) of BP occluded in $Na_{56}FAU$ (1 BP per unit cell).

We have determined the slopes of the regression lines of the MSD according to

$$\langle \Delta R(t)^2 \rangle = 6Dt + a \tag{8}$$

where the parameter a describes the initial sharp rise because of the accessible free volume at the sorption site.[60]

BP/FAU. The instantaneous distances between one O_z atom of the framework and one C atom of the inter-ring bond of BP were indicative of three jumps to neighbor supercages during 1 ns, whereas the instantaneous distances $O_z\cdots H(BP)$ were indicative of large intracage mobility between the intercage jumps. The BP molecule carries out large motions within a supercage and sometimes moves to another neighbor supercage. In addition, the instantaneous dihedral angular values provide evidence of a 10° average rotational motion around the mean value (50°) and sometimes a rapid rotation of 80° (or −280°) to 130°. The BP MSDs were calculated from the trajectory file of extended MD simulations (Figure 9), and the self-diffusivity D value of 1 BP in FAU was found to be $\sim 2 \times 10^{-11}$ $m^2 s^{-1}$.

BP/M_{56}FAU (M^+ = Na^+, K^+, or Cs^+). The instantaneous distances between one O_z atom of the framework and one C atom of the inter-ring bond of BP were indicative of six jumps to neighboring supercages during 1 ns, whereas the instantaneous distances $O_z\cdots H(BP)$ were indicative of lower intracage mobility between the intercage jumps. In addition, the instantaneous dihedral angular values provide evidence of a 10° average rotational motion around the mean value (50°) and sometimes a rapid rotation of 80° (or −280°) to 130°.

In our modeling conditions, the estimates of diffusion coefficients of benzene in siliceous FAU and $Na_{56}FAU$—10^{-10} and 10^{-11} m^2 s^{-1}, respectively—were found to be in reasonable agreement with the ^2H NMR experimental values—4×10^{-10} and 4×10^{-12} m^2 s^{-1}, respectively—as well as earlier calculated values.[14] With the same force field, charges, and calculation conditions, the BP self-diffusion yields unexpected results. Indeed, the coefficients are found to be 2×10^{-11} and 2×10^{-10} m^2 s^{-1} in FAU and $Na_{56}FAU$, respectively. In the absence of an experimental counterpart, it appears after several attempts that at low coverage (1 BP/UC), (i) the BP diffusion is slower than that of benzene in FAU, (ii) the BP diffusion is faster than that of benzene in $Na_{56}FAU$, and (iii) the BP diffusion is faster in $Na_{56}FAU$ than in FAU. The unexpected dynamic behavior is attributed to the BP structure and flexibility in the sorption site: BP lies with one phenyl group facially coordinated to the SII cations and the other phenyl group engaged in the 12-ring windows. The energy barrier to pass the window appears to be low because the phenyl group engaged in the window can migrate to the SII cation site of the neighbor cage concomitantly with the migration of the phenyl group from the SII site to the window without marked change of the energy (Figure 4).

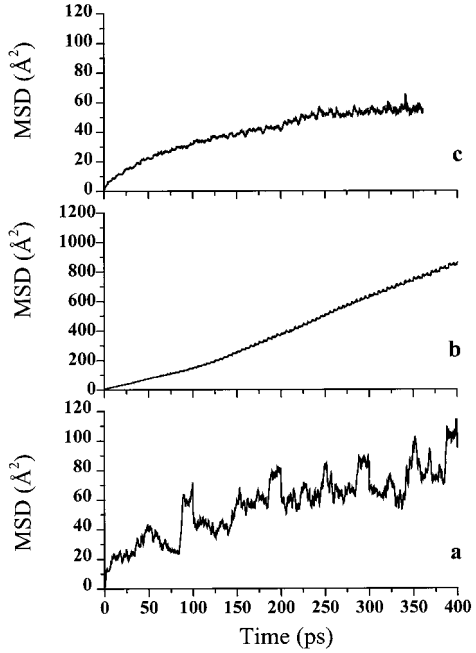

Figure 9. Ensemble average of the mean-square displacements at 300 K of BP occluded in (a) 1 BP/FAU, (b) 1 BP/$Na_{56}FAU$, and (c) 8 BP/$Na_{56}FAU$.

As expected from the size of the cation M^+, the BP MSD obtained from MD simulations over 1 ns decrease markedly from $Na_{56}FAU$, $K_{56}FAU$, and $Cs_{56}FAU$, Figure 10. The decrease of the value of diffusion coefficient from 2×10^{-10}, 5×10^{-11}, and 10^{-11} m^2 s^{-1}, according to the increased sizes of the extraframework cations, are indicative of the restriction on the BP mobility in the void space.

The average D value decreases markedly as the loading increases. This decreasing of the self-diffusivity can be correlated to BP pair occupancy in supercages (Figure 9). The MSD of individual BP was found to be dramatically higher than the

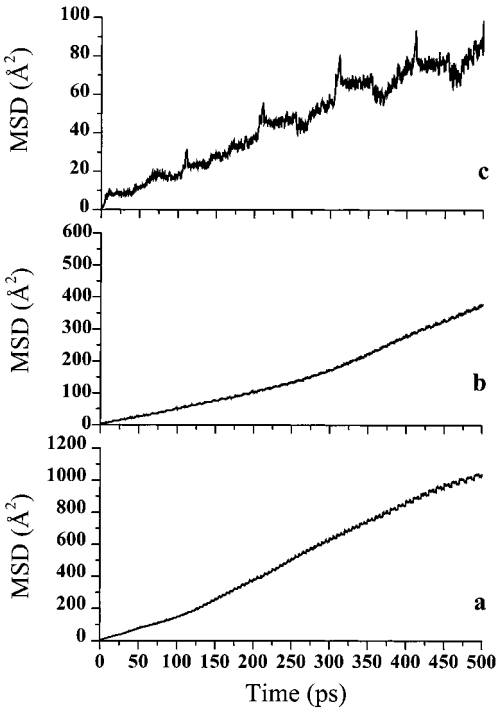

Figure 10. Ensemble average of the mean-square displacements at 300 K of BP occluded in (a) 1 BP/Na_{56}FAU, (b) 1 BP/K_{56}FAU, and (c) 1 BP/Cs_{56}FAU.

MSD of BP in pairs, and the instantaneous BP···BP distances (5 Å) were found to be indicative of the stability of the pairs over the simulation time.

4. Structures and Spectroscopic Behavior of BP in Solution and in the Solid State. Biphenyl and its derivatives have been extensively studied experimentally and theoretically to investigate their molecular structures and spectroscopic properties. BP molecular structure has been reported to be twisted (42°) in the gas phase,[46] in solution, and in the melt.[47] The planar conformation given by X-ray diffraction data recorded at temperatures above 40 K would correspond to a nonequilibrium molecular structure.[48] On the contrary, in the crystal below 40 K, nonplanar structures were found. This change of geometry was expected to affect the excitation energies in addition to the normal effect of the media, which must be kept in mind when comparing the experimental and theoretical data.

The UV−visible absorption, infrared absorption, and Raman scattering properties of BP are well documented. A prominent band was observed at 250 nm in the UV−visible BP spectrum recorded in solution. This band was assigned to the $S_3 \leftarrow S_0$ ($\pi^* \leftarrow \pi$) electronic transition. The electronic absorption spectrum of BP in the bulk state is somewhat different from that of the solution, and the supplementary band detected near 300 nm can be assigned to the planar conformation in the solid state.[62]

The assignment of the Raman and IR features of the BP in solution with twisted conformation was performed previously.[54,63] The isolated BP with D_2 molecular symmetry group has $15A + 16B_1 + 16B_2 + 13B_3$ fundamental vibrational modes: A, B_1, B_2, and B_3 are Raman active, whereas only B_1, B_2, and B_3 are infrared active. Two Raman features were detected in the C−H stretching range at 3070 and 3040 cm^{-1}.[54,63] The two prominent Raman bands at 1615 (A) and 1595 cm^{-1} (B_1) are derived from the 8a and 8b modes of phenyl group, respectively. These bands were assigned to C−C stretches and ring planar deformations.[54] The band at 1285 cm^{-1} (A) was assigned to the stretching of the inter-ring C−C bond of BP. The corresponding bands were observed at 1605, 1590, and 1275 cm^{-1} for BP in the bulk state derive from the Raman active modes A_g, B_{1g}, and A_g of the planar molecule (D_{2h}), respectively. No apparent band splitting (A_g or B_g) through dynamic effect in the solid state with the C_{2h} factor group and 2 BP/UC is detected for any molecular mode in the powder Raman spectra recorded at room temperature.

The most prominent IR bands were observed at 1480 (B_3) and 1424 cm^{-1} (B_2) for the BP in solution, whereas in the solid state, the most intense bands were detected at 1480, 1430, and 1345 cm^{-1} and derive from the IR active modes B_{3u}, B_{2u}, and B_{2u} of the planar molecule, respectively.[54]

5. BP Sorption into M_nFAU Zeolites ($n = 0$ or 56 and M = Na^+, K^+, or Cs^+). Solid BP exhibits vapor pressure too weak at room temperature to undertake the sorption procedure through sublimation from a compartment containing the solid BP to another compartment containing the freshly dehydrated zeolite sample even under gentle warming.[35] The adsorption from BP solution in organic solvent can be an alternative to avoid this problem. However, then it is difficult to eliminate the solvent from the void space without damaging the sample. The method used was the mixture under dry argon of weighted amounts of dehydrated zeolite with 1−2 μm crystal size and dry pure BP in the same reactor. The cell was allowed to stand at 60 °C for several weeks until the sorption of guest molecules into the void space of the zeolites went to completion. The sorption process was monitored as a function of time by diffuse reflectance UV−visible absorption spectrometry at different loadings.

When the diffuse reflectance UV−visible absorption spectra were recorded immediately after the rapid mixing and shaking of the powders, the absorption features were found to be typical of the BP bulk state. Progressively, the absorption in Kubelka−Munck units evolved from the characteristics of the bulk state to an intense absorption with a good resemblance in shape with BP in solution. However, the absorption increased dramatically with time and went to completion after one month.

Before any spectrometric investigation of BP sorbed in faujasitic Y zeolites, we evacuated the samples for 1 h under vacuum to remove the remaining BP adsorbed on the external surface of the crystals. Then the samples were allowed to stand in the cells several weeks at 50 °C under argon to obtain well-equilibrated samples.

6. Spectroscopic Investigations of BP occluded in M_nFAU zeolites ($n = 0$ or 56 and M = Na^+, K^+, or Cs^+). *6.1. Raman Scattering and IR Diffuse Reflectance Spectrometries. BP/FAU.* The Raman and IR features attributed to the host were found to be practically insensitive to the presence of BP in the void space of BP even at high loading. The Raman and IR bands of occluded BP were found to be typical of the BP molecule in solution with twisted conformation and D_2 symmetry. The wavenumbers and the relative intensities of the corresponding Raman and IR features of BP occluded in FAU and in cyclohexane solution were found to be closely analogous (Figure 11).[63] The C−H bond motions are expected to be affected by the surrounding environment. Unfortunately, the Raman scattering and IR absorption features of C−H stretching modes broaden slightly upon sorption with respect to the solution features, and no significant conclusion can be drawn. In addition, no significant wavenumber shifts and relative intensity changes were detected upon increases in the loading values from 1 BP/FAU to 8 BP/FAU, and no direct analogy was found with the solid state.

The sorption undergoes isotropic and weak perturbation of the D_2 symmetry that results in weak spectral shifts and band

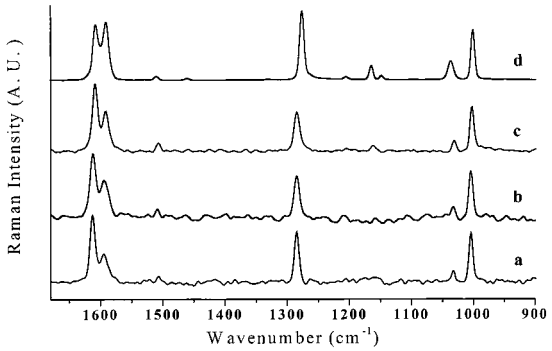

Figure 11. FT-Raman spectra at room temperature of BP (a) in cyclohexane solution, (b) occluded in siliceous FAU (2 BP/FAU), (c) occluded in Na_{56}FAU (2 BP/Na_{56}FAU, and (d) in the bulk solid state.

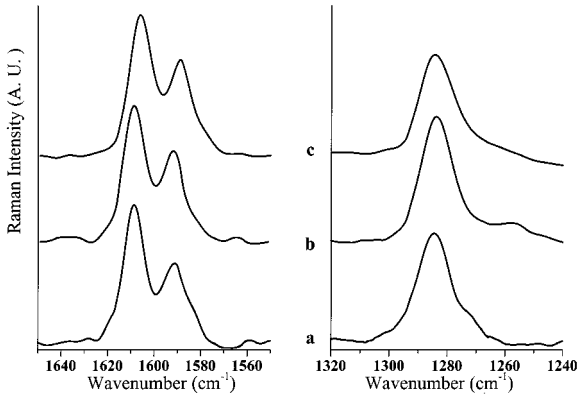

Figure 12. FT-Raman spectra in the 1650−1550 and 1320−1240 cm^{-1} ranges at room temperature of BP (a) occluded in Na_{56}FAU (2 BP/Na_{56}FAU), (b) occluded in K_{56}FAU (2 BP/K_{56}FAU), and (c) occluded in Cs_{56}FAU (2 BP/K_{56}FAU).

broadening. The similarity between the BP vibrational spectra in solution and occluded in siliceous FAU provides clear evidence that the motion of BP approaches at room temperature the rapid isotropic limit characteristic of a liquid. Particularly, the wavenumber (1285 cm^{-1}) and bandwidth (10 cm^{-1}) of the Raman band assigned to the stretching of the inter-ring C−C bond of BP in FAU were found to exhibit remarkable similarities with the C−C calculated vibrational density of states of occluded BP (see section 3.2)

M_{56}FAU ($M^+ = Na^+$, K^+, or Cs^+). In aluminated faujasite Na_{56}FAU, the intrazeolite electrostatic field does not promote marked wavenumber and intensity changes of the IR and Raman features of BP upon sorption at low coverage. So the Raman and IR bands were found to be typical of the BP twisted structure and D_2 local symmetry. The Raman scattering and IR absorption features of C−H stretching modes broaden slightly upon sorption with respect of the solution features, but no significant conclusion with respect of the sorption site can be drawn. In the case of bulky cations such as K^+ and Cs^+, no supplementary band splitting or marked broadening appears, and only weak frequency shifts were detected in Figure 12. The Raman and IR features attributed to the hosts were found to be practically insensitive to the presence of BP in the void space of BP even at high loading.

Increased BP loading in Na_{56}FAU from 1 to 16 BP/UC causes weak wavenumber shifts and weak broadening of the most prominent Raman and IR features. In addition, the intensities of all the Raman bands were found to be proportional to the bulk coverage value (Figure 13). The Raman scattering and IR absorption features of C−H stretching modes only broaden

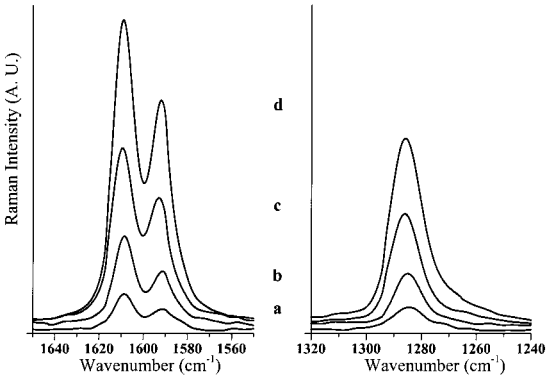

Figure 13. FT-Raman spectra in the 1650−1550 and 1320−1240 cm^{-1} ranges at room temperature of BP occluded in Na_{56}FAU as a function of the loading of (a) 1 BP/Na_{56}FAU, (b) 2 BP/Na_{56}FAU, (c) 4 BP/Na_{56}FAU, and (d) 8 BP/Na_{56}FAU.

slightly at high coverage with respect of the features shown at low coverage. No direct analogy was found with the solid state.[63]

The similarity between the BP vibrational spectra in solution and occluded in M_{56}FAU provides clear evidence that the motion of BP approaches at room temperature the rapid isotropic limit characteristic of a liquid even at high coverage. Particularly, the wavenumber (1285 cm^{-1}) and bandwidth (10 cm^{-1}) of the Raman band assigned to the stretching of the inter-ring C−C bond of BP in Na_{56}FAU were found to exhibit remarkable similarities with the C−C calculated vibrational density of states of occluded BP (see section 3.2). In the time scale of the vibrational spectroscopy (10^{-12} s), the BP rapid motions at room temperature average the environment effect and vibrational coupling when supercages are filled with 2 BP at high coverage.

6.2. UV−Visible Diffuse Reflectance Spectrometry. BP/FAU. The UV−visible absorption spectra of the BP occluded in siliceous FAU (2 BP/UC) displays an intense symmetric band centered at 238 nm. The blue shift with respect of the solution spectrum can be attributed to the isotropic perturbation generated by the surrounding oxygen atoms of the internal surface. Increased BP loading causes no distinct wavelength shift, but the increase of the intensity (Kubelka−Munk units) is found to be less than proportional to the bulk loading value. This fact is attributed to BP−BP interactions in the exited states. However, no significant conclusion with respect to the BP aggregation can be drawn.

M_{56}FAU ($M^+ = Na^+$, K^+, or Cs^+). The UV−visible absorption spectra of the BP occluded in M_{56}FAU (1 BP/UC) display an intense symmetric band centered around 250 nm. The intracavity electrostatic field promotes weak red shifts with respect to the solution spectrum. In contrast, increased BP loading in Na_{56}FAU generates marked absorption wavelength shifts and band shape changes. In addition, the dependence between the absorption intensity (in Kubelka−Munk units) and bulk loading value diverges dramatically from the linearity (Figure 14).

The UV−visible absorption behavior can provide an experimental evidence of the aggregation and average distribution of BP in the void space. The isolated BP in the void space (1 BP/UC) exhibits a strong oscillator strength for the $S_3 \leftarrow S_0$ electronic transition. The aggregation promotes a dramatic decrease of the oscillator strength in the corresponding wavelength range. It is difficult to give a quantitative interpretation of the data, but the absorption value is very sensitive to the aggregation and indicates some pairs even at relatively low coverage and a heterogeneous BP occupation of the supercage. The association of BP molecules in excited states should be

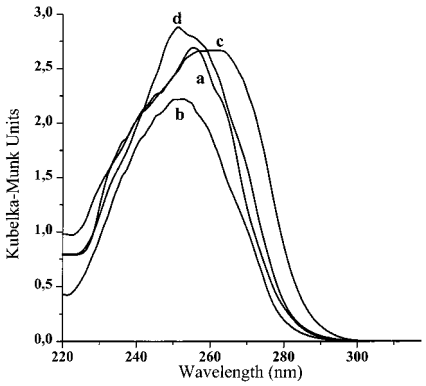

Figure 14. Diffuse reflectance UV−visible absorption spectra at room temperature of BP occluded in $Na_{56}FAU$ as a function of the loading of (a) 1 BP/$Na_{56}FAU$, (b) 2 BP/$Na_{56}FAU$, (c) 4 BP/$Na_{56}FAU$, and (d) 8 BP/$Na_{56}FAU$.

taken into account to interpret the electronic absorption behavior. Thus, excimer formation of entrapped preaggregated aromatics was invoked previously to explain the fluorescence emission.[64] The association between BP molecules at relatively low coverage was pointed out by the modeling results (see section 1). For example, at a bulk concentration of 8 BP/UC corresponding to an average occupancy of 1 BP per supercage, there are supercages with 2 BP, supercages with 1 BP, and empty supercages. As the BP loading increases, the amount of supercages filled by 2 BP per supercage increases, and the 2 BP supercage occupancy was not found to hardly depend on time at the nanoseconde time scale (see section 3.3).

7. Spectroscopic Investigations of BP Occluded under Vacuum, under O Atmosphere, and with Water in $Na_{56}FAU$ Zeolite. All the above spectroscopic investigations were carried out with strictly dehydrated samples and under argon. The BP loading of zeolite under oxygen did not generate significant changes in the Raman and UV−visible absorption spectra. The conformation, siting occupation, and distribution of BP throughout the void space under oxygen and argon are analogous for equilibrated samples and corresponding coverages. It should be noted that the gas change of the cell through vacuum evacuation did not provide equilibrated samples. An equilibration period of several weeks is found to be necessary before any suitable UV-visible absorption measurements to be made.

The introduction of small amounts of water (16 H_2O/UC) in several dehydrated samples did not promote any conformation or siting location changes that could bee seen from the Raman spectra. However, even after a long equilibration time, the UV−visible spectra indicate some changes in the BP occupation of the supercages, particularly at high BP loading.

Conclusions

The Monte Carlo simulations at 300 K indicate the energetically favored locations of BP in the void space of M_nFAU (n = 0 or 56 and $M^+ = Na^+$, K^+, or Cs^+) zeolites as a function of BP loading. No preferential site is determined in purely siliceous FAU, whereas well-defined location sites energetically favored are effective in $M_{56}FAU$ aluminated faujasite with extraframework cations. The formation of BP bimolecular aggregates within the same supercage occurs from 2 BP/M_n-FAU and more average loading. This latter finding is in agreement with the value deduced from UV−vis absorption experiments.

The energy minimization procedure indicates that in the lowest-energy site, BP lies in the $M_{56}FAU$ cavity in a twisted conformation with one phenyl group facially coordinated to the SII cations and the other phenyl group engaged in the 12-ring windows. The accommodation of 2 BP per supercage does not change the sorption site as well as the twisted conformation. The structure and the flexibility of the BP molecule can explain this striking diffusion behavior in the void space of the faujasitic zeolites.

The molecular dynamics calculations provide evidence of the BP intra- and intercage mobility. Surprisingly, the presence of Na^+ cations in the available void space of $Na_{56}FAU$ does not hinder the BP diffusion with respect to the diffusion in purely siliceous FAU. Nevertheless, the presences of bulkier cations such as Cs+ reduce markedly the molecular displacement.

The formation of BP aggregates within the same supercage at high loading reduced again the molecular mobility. The Fourier transformation of the velocity autocorrelation function provides the vibrational density of states of the atoms of framework, Na^+ and BP. The calculated frequency values are in reasonable agreement with the frequency values deduced from Raman and IR bands. The structure of the zeolite hosts remains practically unchanged upon BP sorption even at high coverage, whereas the preferred BP conformation is found to be twisted. In the time scale of the vibrational spectroscopy, the occluded BP exhibits marked flexibility and mobility at room temperature. The presence of gases and low water content does not change markedly the occupation sites and the conformation of occluded BP.

Acknowledgment. The authors are very grateful to Dr. A. Moissette and Dr. B. Sombret for their assistance and advice on the FT-Raman and diffuse reflectance IR absorption spectrometries. The authors acknowledge Dr. D. Bougeard for helpful discussions. The Centre d' Etudes et de Recherches Lasers et Applications (CERLA) is supported by the Ministère chargé de la recherche, the région Nord/Pas de Calais, and the Fonds Européen de Développement Economique des Régions.

References and Notes

(1) Mao, Y.; Thomas, J. K. *J. Chem. Soc., Faraday Trans.* **1992**, *88*, 3079.
(2) Thomas, J. K. *Chem. Rev.* **1993**, *93*, 301.
(3) Ramamurthy, V.; Lakshminarasimhan, P.; Grey, C. P.; Johnston, L. J. *J. Chem. Soc., Chem. Commun.* **1998**, 2411.
(4) Yoon, K. B. *Chem. Rev.* **1993**, *93*, 321.
(5) Brémard, C.; Buntinx, G.; De Waele, V.; Didierjean, C.; Gener, I.; Poizat, O. *J. Mol. Struct.* **1999**, *480−481*, 69.
(6) Gener, I.; Buntinx, G.; Brémard, C. *Angew. Chem., Int. Ed. Engl.* **1999**, *38*, 1819.
(7) Dzhigit, O. M.; Kiselev, A. V.; Rachmanova, T. A. *Zeolites* **1984**, *4*, 389.
(8) Ruthven, D. M.; Goddard, M. *Zeolites* **1986**, *6*, 275.
(9) Fitch, A. N.; Jobic, H.; Renouprez, A. *J. Phys. Chem.* **1986**, *90*, 1311.
(10) Czjzek, M.; Vogt, T.; Fuess, H. *Zeolites* **1991**, *11*, 882.
(11) Czjzek, M.; Fuess, H.; Vogt, T. *J. Phys. Chem.* **1991**, *95*, 5255.
(12) Mellot, C.; Espinat, D.; Rebours, B.; Baerlocher, C.; Fisher, P. *Catal. Lett.* **1994**, *27*, 159.
(13) Parize, L. M.; Hriljac, J. A.; Cox, D. E.; Corbin, D. R.; Ramamurthy, V. *J. Chem. Soc., Chem. Commun.* **1993**, 226.
(14) Bull, L. M.; Henson, N. J.; Cheetham, A. K.; Newsam, J. M.; Heyes, S. J. *J. Phys. Chem.* **1993**, *97*, 11776.
(15) Hong, S. B.; Cho, H. M.; Davis, M. E. *J. Phys. Chem.* **1993**, *97*, 1629.
(16) Sousa Gonsalves, J. A.; Portsmouth, R. L.; Alexander, P.; Gladden, L. F. *J. Phys. Chem.* **1995**, *99*, 3317.
(17) Zibrowius, B.; Caro, J.; Pfeifer, H. *J. Chem. Soc., Faraday Trans 1* **1998**, *84*, 2347.
(18) Kirschhock, C.; Fuess, A. *Microporous Mater.* **1994**, *2*, 261.
(19) Jobic, H.; Renouprez, A.; Fitch, A. N.; Lauter, H. *J. Chem. Soc., Faraday Trans 1* **1987**, *83*, 3199.
(20) Jobic, H.; Bee, M.; Kearley, G. J. *Zeolites* **1992**, *12*, 146.
(21) Unland, M. L.; Freeman, J. J. *J. Phys. Chem.* **1978**, *54*, 183.

(22) De Mallmann, A.; Barthomeuf, D. *Zeolites* **1988**, *8*, 292.
(23) Coughlan, B.; Keane, M. A. *J. Chem. Soc., Faraday Trans*. **1990**, *86*, 3961.
(24) O'Malley, P. J. *Chem. Phys. Lett.* **1990**, *166*, 340.
(25) Freeman, M. L.; Unland, M. L. *J. Catal*. **1978**, *54*, 83.
(26) Catlow, C. R. A. *Modelling of Structure and Reactivity in Zeolites*; Academic Press: London, 1992.
(27) Demontis, P.; Yashonath, S.; Klein, M. L. *J. Phys. Chem.* **1989**, *93*, 5016.
(28) Schrimpf, G.; Schlenkrich, M.; Brickman, J.; Bopp, P. *J. Phys. Chem.* **1992**, *96*, 7404.
(29) Schrimpf, G.; Tavitian, B.; Espinat, D. *J. Phys. Chem.* **1995**, *99*, 10932.
(30) Auerbach, S. M.; Henson, N. J.; Cheetham, A. K.; Metiu, H. I. *J. Phys. Chem.* **1995**, *99*, 10600.
(31) Auerbach, S. M.; Metiu, H. I. *J. Chem. Phys.* **1996**, *105*, 3753.
(32) Klein, H.; Fuess, H.; Schrimpf, G. *J. Phys. Chem.* **1996**, *100*, 11101.
(33) Mosell, T.; Schrimpf, G.; Brickman, J. *J. Phys. Chem.* **1997**, *101*, 9476.
(34) Mosell, T.; Schrimpf, G.; Brickman, J. *J. Phys. Chem.* **1997**, *101*, 9485.
(35) Brémard, C.; Ginestet, G.; Le Maire, M. *J. Am. Chem. Soc*. **1995**, *117*, 9274 and references therein.
(36) Brémard, C.; Bougeard, D. *Adv. Mater*. **1995**, *7*, 10 and references therein.
(37) Brémard, C.; Le Maire, M. *J. Phys. Chem.* **1993**, *97*, 9695.
(38) Kubelka, P.; Munck, F. *Z. Tech. Phys.* **1931**, *12*, 593.
(39) Brémard, C.; Ginestet, G.; Laureyns, J.; Le Maire, M. *J. Am. Chem. Soc*. **1996**, *118*, 12724.
(40) Hriljac, J. A.; Eddy, M. M.; Cheetham, A. K.; Donohue, J. A.; Ray, G. J. 19 *J. Solid State Chem*. **1993**, *106*, 66.
(41) Eulenberger, G. R.; Shoemaker, D. P.; Keil, J. G. *J. Phys. Chem.* **1967**, *71*, 1812.
(42) Uytterhoeven, L.; Dompas, D.; Mortier, W. J. *J. Chem. Soc., Faraday Trans*. **1992**, *3*, 633.
(43) Loewenstein, W. *Am. Mineral.* **1954**, *39*, 92.
(44) Ghermani, N. E.; Lecomte, C.; Dusausoy, Y. *Phys. Rev. B* **1998**, *53*, 5231.
(45) Almeningen, A.; Bastiansen, O.; Fernholt, L.; Cyvin, B. N.; Cyvin, S. J.; Samdal, S. *J. Mol. Struct.* **1986**, *128*, 59.
(46) Schmid, E. D.; Brosa, B. *J. Chem. Phys.* **1972**, *56*, 6267.
(47) Barrett, R. M.; Steele, D. *J. Mol. Struct.* **1972**, *11*, 105.
(48) Charbonneau, G. P.; Delugeard, Y. *Acta Crystallogr*. **1976**, *B 32*, 1420.
(49) Negri, F.; Zgierski, M. Z. *J. Chem. Phys.* **1992**, *97*, 7124.
(50) Lee, S. Y. *Bull. Korean Chem. Soc*. **1998**, *19*, 93, and references therein.
(51) Ermoshin, V. A.; Smirnov, K. S.; Bougeard, D. *Chem. Phys*. **1996**, *202*, 41.
(52) Ermoshin, V. A.; Smirnov, K. S.; Bougeard, D. *Chem. Phys*. **1996**, *209*, 53.
(53) Rappé, A. K.; Goddard, W. A., III. *J. Phys. Chem.* **1991**, *95*, 3358.
(54) Zerbi, G.; Samdroni, S. *Spectrochim. Acta* **1968**, *24A*, 483.
(55) Boumiz, A.; Cartigny, J.; Cohen de Lara, E. *J. Phys. Chem*. **1992**, *96*, 5419.
(56) Mayo, S. L.; Olafson, B. D.; Goddard, W. A. III. *J. Phys. Chem*. **1990**, *94*, 8897.
(57) Rappé, A. K.; Casevit, C. J.; Colwell, K. S.; Goddard, W. A. III.; Skiff, W. M. *J. Am. Chem. Soc*. **1992**, *114*, 10024.
(58) Lachet, V.; Boutin, A.; Tavitian, B.; Fuchs, A. *J. Phys. Chem*. **1998**, *102*, 9224.
(59) Sprik, M.; Klein, M. L. *Chem. Phys.* **1988**, *89*, 7556.
(60) Henson, N. J.; Cheetham, A. K.; Stockenhuber, M.; Lercher, J. A. *J. Chem. Soc., Faraday Trans.* **1998**, *94*, 3759.
(61) Nicholson, J. B.; Hay, B. P.; Dixon, D. A. *J. Phys. Chem. 1999*, *103*, 1394.
(62) Rubio, M.; Merchan, M.; Orti, E.; Roos, B. O. *Chem. Phys. Lett*. **1995**, *234*, 373.
(63) Bree, A.; Pang, C. Y.; Rabenek, L. *Spectrochim. Acta* **1971**, *27A*, 1293.
(64) Ramamurthy, V.; Sanderson, D. R.; Eaton, D. F. *J. Phys. Chem.* **1993**, *97*, 13380.